Proceedings of the ICBBG2025
2025 International conference on Bio-mediated and Bio-inspired Geotechnics
18-20 May, 2025 | Tempe, Arizona, USA
https://doi.org/10.53243/ICBBG2025-58

Design Considerations for Multi-axial Tensile Testing of Conventional and Next-Generation Geosynthetic Specimens

Emre Duman,[1] J. David Frost[2]

[1]Graduate Research Assistant, School of Civil & Environmental Engineering, Georgia Institute of Technology, Atlanta, GA, 30332, USA
[2]Professor, School of Civil & Environmental Engineering, Georgia Institute of Technology, Atlanta, GA, 30332, USA.

ABSTRACT

Geosynthetics, and in particular geogrids, have been used as stabilization and reinforcement in various geotechnical engineering applications such as pavements, retaining walls, and embankments. For pavement applications, radial stiffness is important due to the three-dimensional nature of wheel loading. Traditional products, such as commercially available uniaxial and biaxial geogrids exhibit lower stiffness in non-rib directions than in rib directions, which is not ideal for distributing wheel loading. Therefore, multi-axial directional geogrids have emerged in the market. In addition, manufacturers and researchers have recently introduced next-generation geogrids with multiple opening sizes including spider-web inspired geogrids, amongst other factors. Considering the multi-axial variable opening geometry, it is essential to identify the radial tensile properties of these materials. In practice, manufacturers and designers perform uniaxial tensile tests to characterize the strength and stiffness of geogrids. However, this loading condition does not represent multi-axial in-plane loading due to applied wheel loading. Therefore, it is crucial to investigate geogrids' multi-axial tensile properties appropriately. The work presented herein represents the first step towards a more holistic approach to multi-axial tensile testing. Specifically, careful design of the test specimen to ensure uniform stress and strain conditions are created is crucial. Finite Element Analysis (FEA) is thus performed for multi-axial tensile testing on triaxial geogrids, and the resulting stress-strain distribution is analyzed for different specimen configurations.

INTRODUCTION

Geogrids are polymer structures widely used in geotechnical engineering applications for stabilization and reinforcement. Over the years, various types of geogrids have been manufactured, such as uniaxial, biaxial, and triaxial. The evolution of geogrids involved altering the rib directions and incorporating ribs in multiple directions to achieve higher stiffness across different orientations. In recent years, geogrid designs have evolved significantly, moving from traditional hexagonal unit cell structures with triangular openings to more complex configurations incorporating hexagonal, trapezoidal, and triangular openings. These advancements aim to enhance the mechanical performance of geogrids in stabilization applications. Building upon this progress, researchers have explored bio-inspired designs, such as spider-web-inspired geogrids, to replicate the efficient load distribution and resilience found in natural systems (Peralta et al., 2019; Frost & Oner, 2024). Such bio-inspired approaches embody the principles of bio-inspired

geotechnics, emphasizing sustainable and innovative engineering solutions. The specimens in this study represent "next-generation" multi-axial geogrids because they incorporate these bio-geo-inspired design principles, aiming to achieve superior interaction with aggregate materials and enhanced performance in geotechnical applications.

The multi-axial geogrid test concept can be particularly important in pavement applications, where wheel loading induces three-dimensional stress conditions. In such cases, radial stiffness is crucial for determining the extent of lateral confinement in an aggregate layer (Yang, 2012). Traditionally, radial stiffness has been measured through uniaxial tests on specimens cut in different directions. However, this approach does not accurately represent the multi-axial loading conditions encountered in the field. Therefore, a better testing protocol is needed considering the significant effort involved in designing next-generation bio-inspired geogrids.

Multi-axial tensile testing, specifically biaxial tensile testing, has been applied to various materials, such as sheet metals, composites, and polymers (Kodaira et al., 2022; Schemmann et al., 2018; Swanson et al., 1988). The testing methods include controlling the loading paths using internal and/or external pressure in combination with axial loads (Choo & Hull, 1983) or clamping the material along different axes (Carvelli, 2021). One major challenge in biaxial tensile testing is achieving uniform strain and stress distribution to directly obtain the stress-strain relationship from the experiment. Extensive experimental and numerical studies have been conducted to design specimens that achieve homogeneous strain and stress distribution. The most common specimen geometry is cruciform, with modifications to the sleeves, specimen thickness, and corner radii (Deng et al., 2015; Miková et al., 2022; Moncy et al., 2019). Figure 1 shows an example of a biaxial tensile testing specimen, where the sleeves have slots, the central area is thinner than the sleeves, and the corners are rounded. Another challenge is preventing premature failure in the sleeves due to stress concentration at the corners. However, this study will not focus on this issue, as the large strain properties of geogrids are not critical for pavement applications.

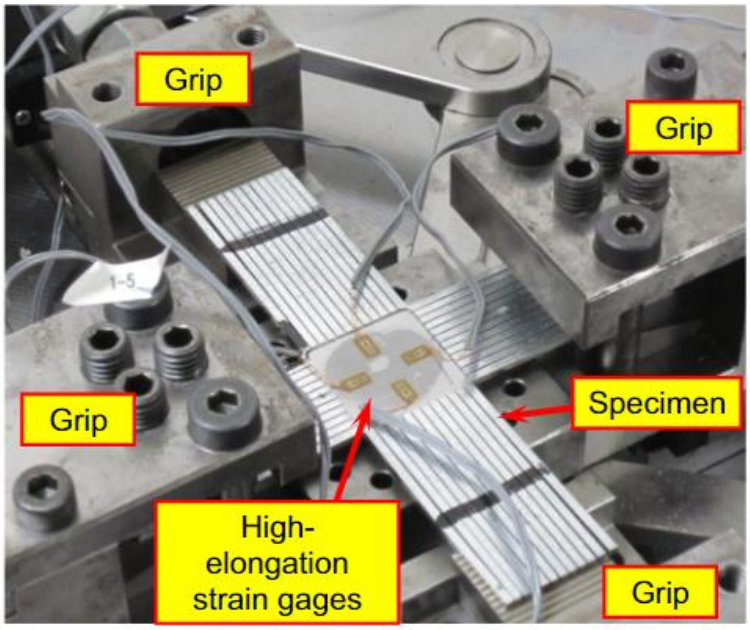

Figure 1. Example biaxial tensile test specimen (Deng et al., 2015)

In this work, preliminary three-dimensional Finite Element Analysis (FEA) was conducted to simulate multi-axial tensile tests on triaxial geogrids. Unlike previous studies, a new loading

path involving three primary loading directions was investigated. The stress and strain distributions were analyzed and presented for specimens with different modifications.

MODEL DESCRIPTION

An elastoplastic material model with isotropic hardening was employed. One of the key features of this model is its ability to represent the nonlinear tensile response of geogrids, as shown in Figure 2. The analysis was conducted using ABAQUS software, which allows the decomposition of elastic and plastic regions. The first step involves converting nominal stress and strain to true stress and strain using Eq 1. and Eq 2.

$$\epsilon_{true} = \ln(1 + \epsilon_{nom}) \qquad Eq.1$$

$$\sigma_{true} = \sigma_{nom}(1 + \epsilon_{true}) \qquad Eq.2$$

where ϵ_{true} is true strain, ϵ_{nom} is nominal strain, σ_{true} is true strain and σ_{nom} is nominal strain. The decomposition of true strain into elastic and plastic components is shown in Figure 3(a).

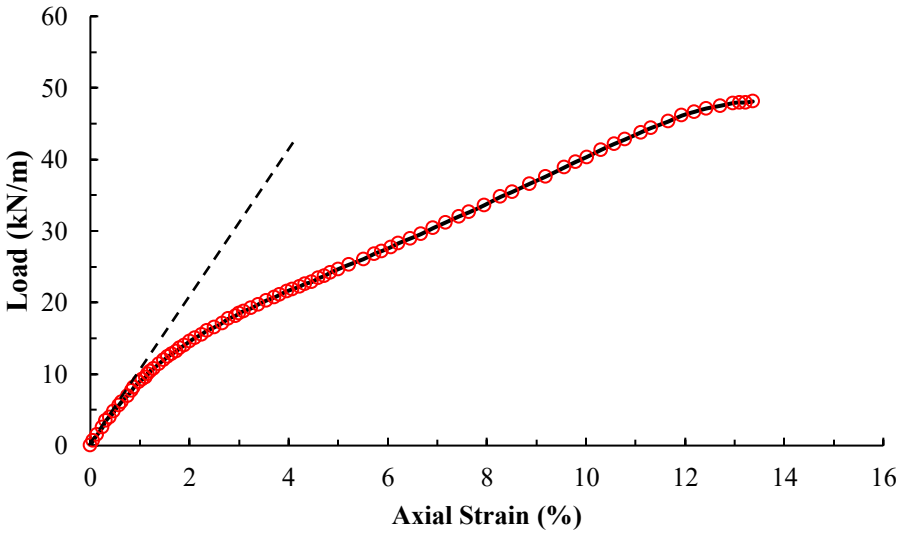

Figure 2. Uniaxial tensile test result

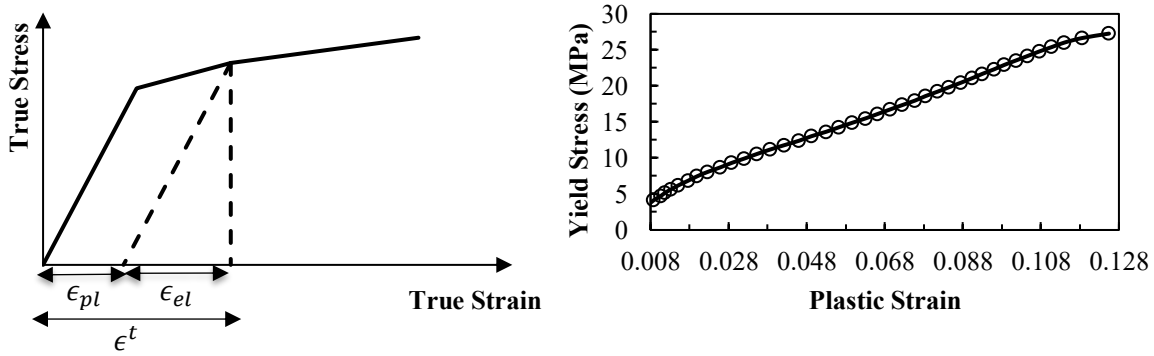

(a) (b)

Figure 3. (a) Elastic and plastic regions (ABAQUS, 2013), (b) yield stress vs. plastic strain for hardening rule

Elastic strain is calculated by Eq. 3.

$$\epsilon_{el} = \frac{\sigma_{true}}{E} \qquad Eq.3$$

where ϵ_{el} is elastic strain, and E is Young's modulus.

The elastic modulus was determined experimentally to be 465 MPa from the experimental result (Figure 2). Poisson's ratio has been reported as 0.3 in several studies (Hussein & Meguid, 2016; Kwon et al., 2008). Yang (2012) analytically calculated Poisson's ratio for triaxial geogrids and reported it as 0.333. In this study, a Poisson's ratio of 0.3 was used. Ongoing work is focused on designing an experimental setup to perform uniaxial, biaxial, and triaxial tensile testing, after which selection of an appropriate Poisson's ratio will be re-evaluated. Additionally, the material was assumed to be isotropic to simplify the model. However, this assumption will also be reviewed after conducting multi-axial tensile tests. Plastic strain is calculated by subtracting elastic strain from true strain. Yield stress vs. plastic strain data (Figure 3b) is provided for hardening rule. Von Mises yield criterion was used for plasticity. The material starts yielding when equivalent von Mises stress (described in Eq 4.) equals to yield stress.

$$\sigma_e = \sqrt{J_2} = \sqrt{\frac{(\sigma_{11}-\sigma_{22})^2 + (\sigma_{22}-\sigma_{33})^2 + (\sigma_{33}-\sigma_{11})^2}{2}} \qquad Eq.4$$

where J_2 is the second invariant of deviatoric tensor.

$$J_2 = \frac{1}{6}[(\sigma_{11}-\sigma_{22})^2 + (\sigma_{22}-\sigma_{33})^2 + (\sigma_{33}-\sigma_{11})^2] \qquad Eq.5$$

The yield function is described in Eq. 6.

$$f(\sigma) = 3J_2 - \sigma_y \qquad Eq.6$$

where σ_y is yield stress.

GEOMETRY AND BOUNDARY CONDITIONS

The simplified geometry and dimensions of the model geogrids are shown in Figure 4(a). Figure 4(b) provides a detailed geometry that more closely resembles an existing manufactured product. In both geometries, the junctions and ribs have a uniform thickness of 2 mm. The detailed geometry includes a fillet, whereas the simplified geometry omits it. A comparison of the FEA results for these geometries is presented in the following sections.

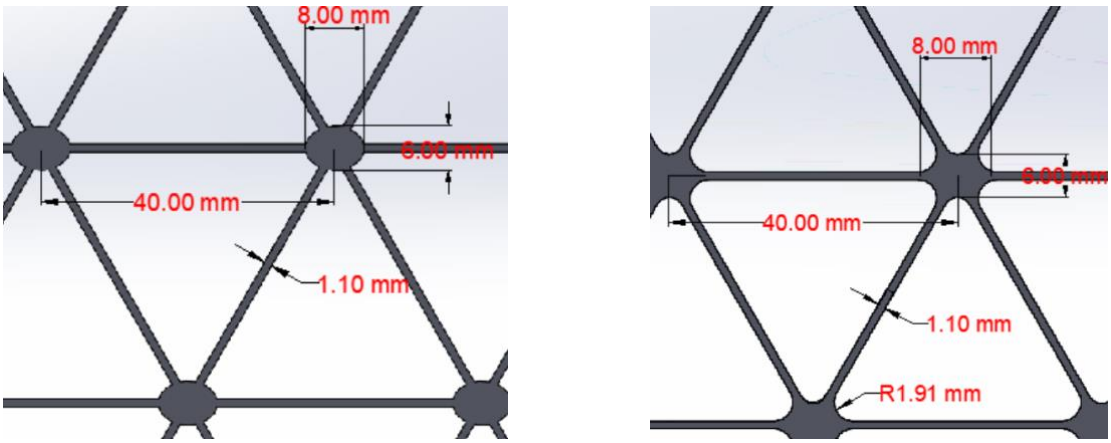

(a) (b)

Figure 4. Geogrid geometry and dimensions. (a) simplified, (b) detailed

The biaxial and triaxial testing specimens with boundary conditions are illustrated in Figures 5a and b. The clamps are assumed to be ideal, allowing no rotation or movement except in the loading direction. Prescribed displacements are applied at a strain rate of 10% per minute. The corresponding displacement rate is calculated using the gauge length of the inner area. The maximum displacement at the clamp locations is 15 mm. Displacements are applied in all directions as described by Hangen et al. (2008) to prevent movement of the specimen's center point, which could otherwise cause distortion and lead to a heterogeneous stress distribution. For meshing, an eight-node brick element with reduced integration (C3D8R) was used. A comparison between the C3D8R and the standard eight-node brick element (C3D8) showed no significant difference in the results. The meshed geometry is shown in Figure 5(c).

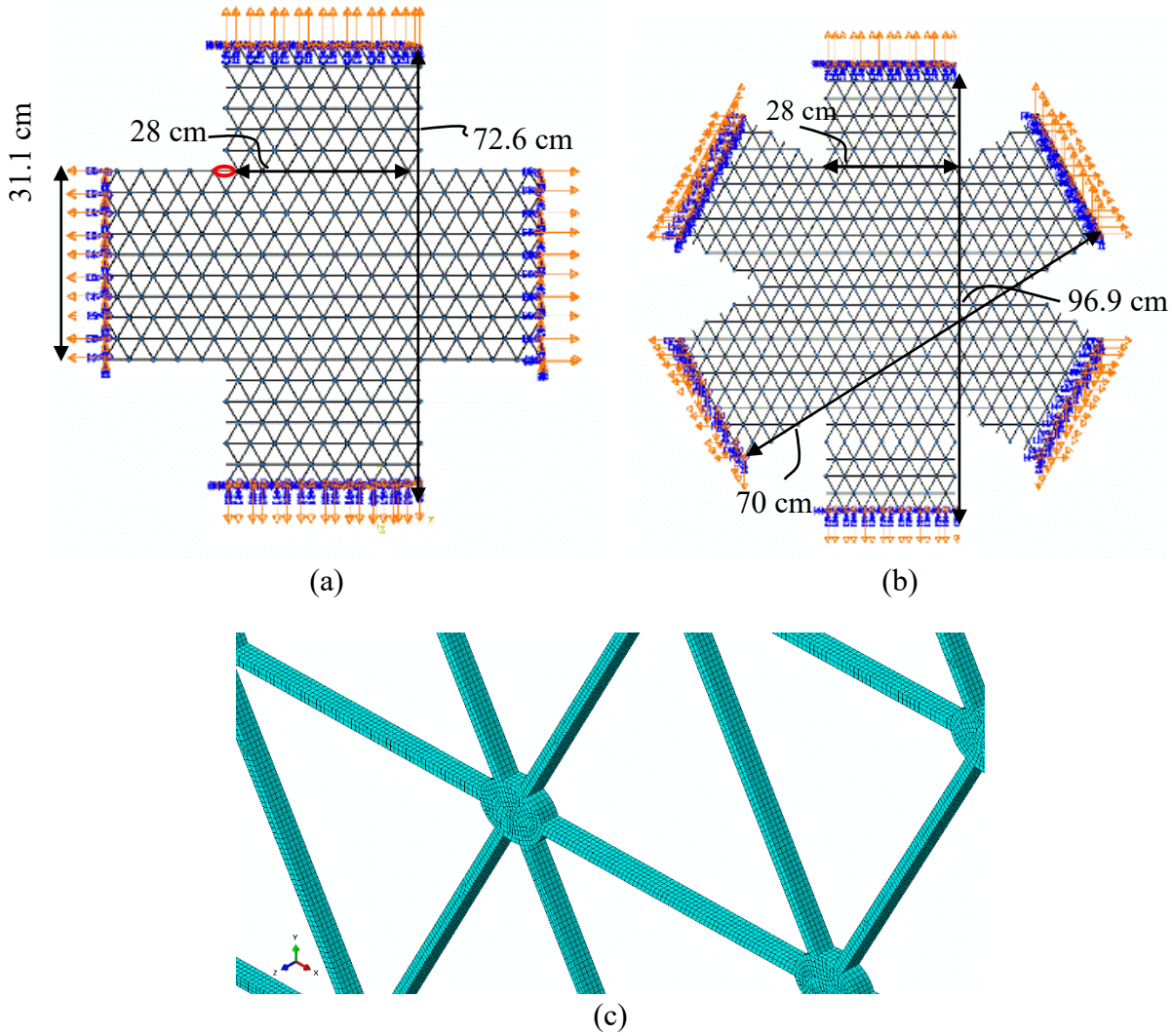

Figure 5. Multi-axial tensile testing specimens, (a) biaxial loading case, (b) triaxial loading case, (c) meshed geometry

RESULTS AND DISCUSSION

The initial investigation focused on the effect of geogrid node geometry. Biaxial tensile tests were simulated for the node geometries shown in Figures 5(a) and 5(b). The horizontal rib at

the upper left corner (highlighted in Figure 5a) was analyzed as it is a location where stress concentration typically occurs. Figure 6(a) shows the vertical displacement profile, while Figure 6(b) presents the equivalent von Mises stress from the center of the left node to the right node. The results indicate that incorporating a radius does not significantly affect the outcome, so the simulations were continued using the simplified geometry.

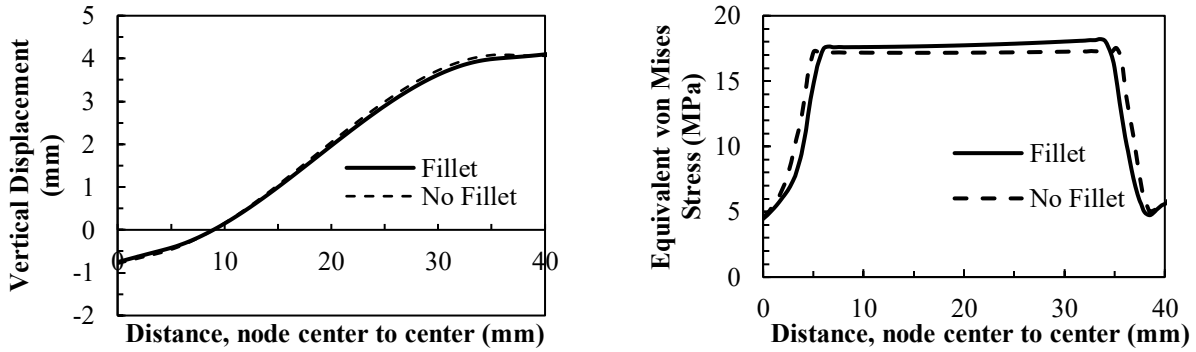

(a) (b)

Figure 6. Comparison of simplified and detailed geometries, (a) Vertical displacement profile, (b) Stress profile

The slot concept from the literature was adopted for the geogrid geometries. Given that the material geometry is grid-like and predefined, there is limited flexibility in modifying features such as corners or thickness. Consequently, inclined or horizontal ribs are often removed in different locations. Figure 7 illustrates the geometries that were investigated. Figure 7(a) shows an unmodified triaxial geometry. The highlighted hexagon represents the region of interest (ROI) where stress distribution was evaluated. Figures 7(b) and 7(c) display modified geometries where rows of inclined ribs perpendicular to the loading directions were removed. This approach was intended to mimic the slotted-arm concept to achieve better stress distribution along the ROI boundaries. Figure 7(d) shows another approach where ribs at the hexagon's boundary were removed. Figure 7(e) presents a further iteration where, in addition to removing the horizontal ribs, the ribs shown in red were also removed. This modification aimed to decouple force transfer between the sleeves. The ROI for this geometry was also adjusted, as highlighted in Figure 7(e). Figure 7(f) is an iteration of the original geometry, but with the ribs connecting the arms removed.

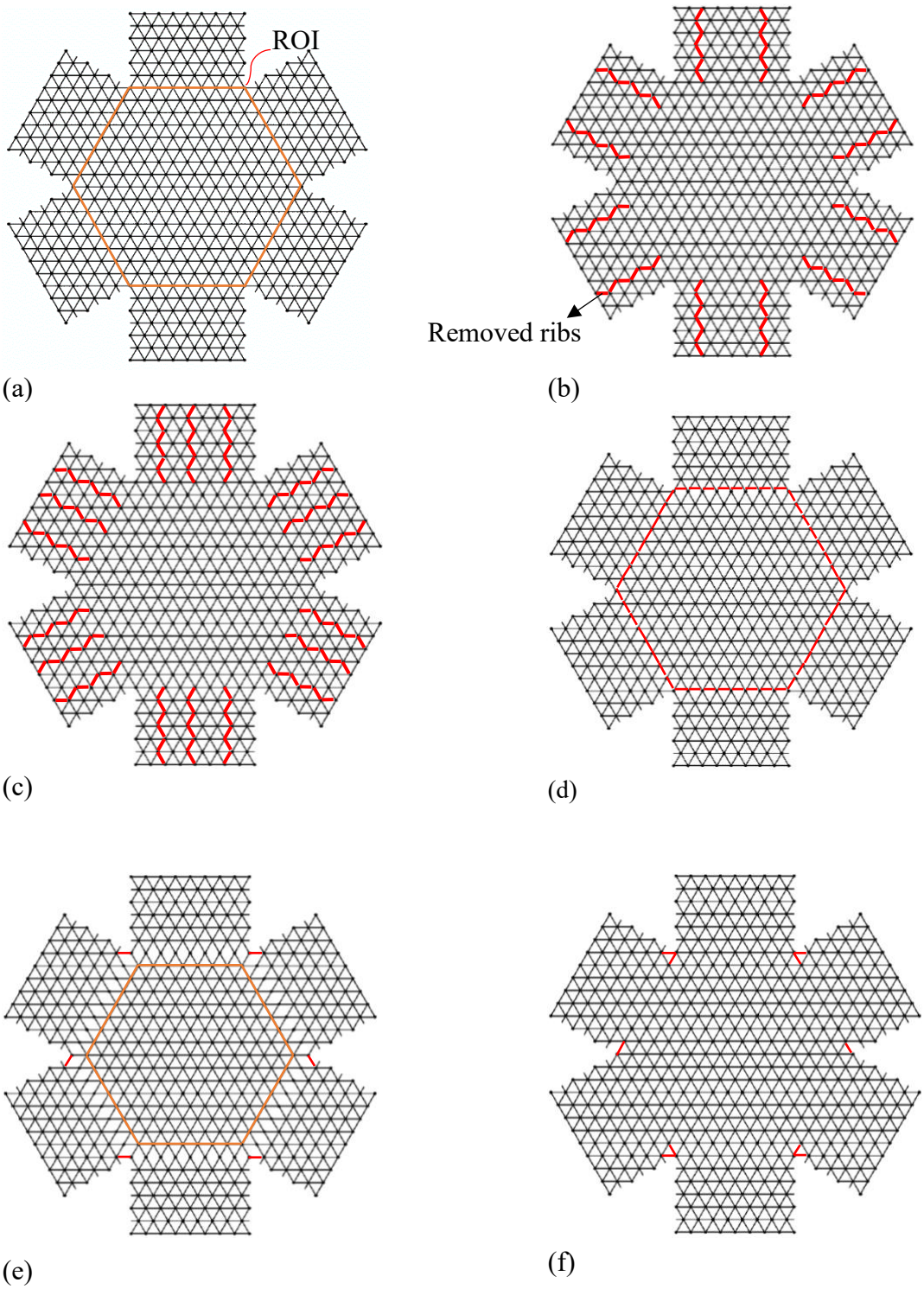

Figure 7. Different specimen geometries for multi-axial tensile testing, (a) baseline geometry, (b) slotted geometry (two rows), (c) slotted geometry (three rows), (d) no ribs at the hexagon level, (e) no ribs at the corner and hexagon level, (f) no ribs at the corner

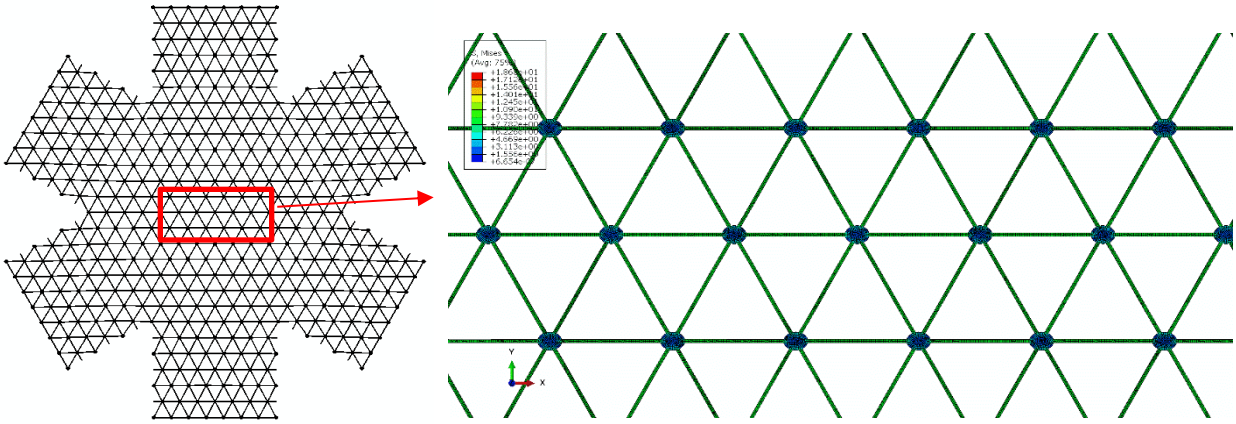

Figure 8. Stress distribution example for reference geometry

Figure 8 shows a screenshot of the stress distribution for the highlighted section in the reference geometry. For each rib (horizontal or inclined), the equivalent von Mises stress at the center of the rib was considered. The average stress and coefficient of variation (COV) of the stress were determined, considering all the ribs within the ROI. For the reference geometry (Figure 7a), the COV was 8.8% and the average stress was 8.8 MPa. This result was used as a baseline for comparison with the modified geometries. The first iterations of the baseline geometry are shown in Figures 7(b) and 7(c), where two and three rows of inclined ribs were removed. The average stresses were 7.83 MPa and 7.30 MPa, respectively, with COVs of 13% in both cases. These results indicate that the slot-like concept worsened the stress distribution and force transfer. In the next case, where the ribs at the hexagon boundary were removed (Figure 7d), the average stress and COV were 9.36 MPa and 12.8%, respectively. An iteration of this geometry (Figure 7e), in which the highlighted ribs were removed to achieve force decoupling between the sleeves, performed better. The average stress was 9.09 MPa, and the COV was 6.8%. Finally, the last geometry (Figure 7f) performed slightly worse than the previous iteration, with an average stress of 9.13 MPa and a COV of 7.2%. Among all the geometries, Figure 7(e) resulted in the lowest COV at 6.8%. Although there is no current standard for multi-axial tensile testing for geogrids, this result suggests a relatively homogeneous stress distribution.

CONCLUSION

Significant effort is required to develop new multi-axial geogrids, including bio-inspired geogrids. However, these new geogrid structures require new testing methods beyond what currently exists. This study presents the initial steps toward specimen design for multi-axial tensile testing of geogrids. A series of FEA simulations were conducted on various geogrid specimens to investigate stress distribution in the ROI. The results indicated that the slit-like concept did not enhance stress distribution. The best performance was achieved by removing the outer ribs at the hexagon's perimeter and the ribs connecting the sleeves. This conclusion is based on the assumption of isotropic material properties. Ongoing work is focused on developing a multi-axial tensile testing apparatus. In the future, with the availability of multi-axial tensile test data, the model can be updated. This study highlights how changes in the geometrical features of the specimen influence stress distribution.

ACKNOWLEDGMENTS

The findings presented in this manuscript are based on work supported by the US National Science Foundation through PTE Federal Award No. EEC-1449501. Any opinions, findings and conclusions or recommendations expressed in this material are those of the authors and do not necessarily reflect the views of the National Science Foundation. Additional funding was provided by the Elizabeth and Bill Higginbotham Professorship in the School of Civil Engineering at Georgia Tech.

REFERENCES

ABAQUS, 2013. ABAQUS User's Manuals, Version 6.13. Dassault Systems Simulia Corp., Providence, RI, USA.

Carvelli, V. (2020). Biaxial tensile behavior of composite reinforcements. In Composite Reinforcements for Optimum Performance (pp. 307–332). Woodhead Publishing. https://doi.org/10.1016/B978-0-12-819005-0.00010-1

Choo, V. K. S., & Hull, D. (1983). Influence of Radial Compressive Stress Owing to Pressure On the Failure Modes of Composite Tube Specimens. Journal of Composite Materials, 17(4), 344–356.

Deng, N., Kuwabara, T., & Korkolis, Y. P. (2015). Cruciform Specimen Design and Verification for Constitutive Identification of Anisotropic Sheets. Experimental Mechanics, 55(6), 1005–1022. https://doi.org/10.1007/s11340-015-9999-y

Hangen, H., Detert, O., & Alexiew, & D. (2008). BIAXIAL TESTING OF GEOGRIDS: RECENT DEVELOPMENTS. 4th European Geosynthetics Conf. EuroGeo4.

Hussein, M. G., & Meguid, M. A. (2016). A three-dimensional finite element approach for modeling biaxial geogrid with application to geogrid-reinforced soils. Geotextiles and Geomembranes, 44(3), 295–307. https://doi.org/10.1016/j.geotexmem.2015.12.004

Kodaira, Y., Miura, T., Takano, Y., & Yonezu, A. (2022). Development of biaxial tensile testing for porous polymer membranes. Polymer Testing, 106(107440). https://doi.org/10.1016/j.polymertesting.2021.107440

Kwon, J., Tutumluer, E., & Konietzky, H. (2008). Aggregate base residual stresses affecting geogrid reinforced flexible pavement response. International Journal of Pavement Engineering, 9(4), 275–285. https://doi.org/10.1080/10298430701582347

Miková, Ľ., Prada, E., Kelemen, M., Krys, V., Mykhailyshyn, R., Sinčák, P. J., Merva, T., & Leštach, L. (2022). Upgrade of Biaxial Mechatronic Testing Machine for Cruciform Specimens and Verification by FEM Analysis. Machines, 10(10), 916. https://doi.org/10.3390/machines10100916

Moncy, A., Castro, O., Berggreen, C., Moncy, A., Castro, O., & Berggreen, C. (2019). Cruciform Specimen Designs For Planar Biaxial Fatigue Testing in Composites. 2nd International Conference on Composite Materials 2019.

Schemmann, M., Lang, J., Helfrich, A., Seelig, T., & Böhlke, T. (2018). Cruciform specimen design for biaxial tensile testing of smc. Journal of Composites Science, 2(1), 12. https://doi.org/10.3390/jcs2010012

Swanson, S. R., Christoforou, A. P., & Colvin, G. E. (1988). Biaxial Testing of Fiber Composites Using Tubular Specimens. Experimental Mechanics, 28, 238–243.

Yang, X. (2012). An assessment of the geometry effect of geosynthetics for base course reinforcements. International Journal of Transportation Science and Technology, 1(3), 247–257.

INTERNATIONAL SOCIETY FOR
SOIL MECHANICS AND
GEOTECHNICAL ENGINEERING

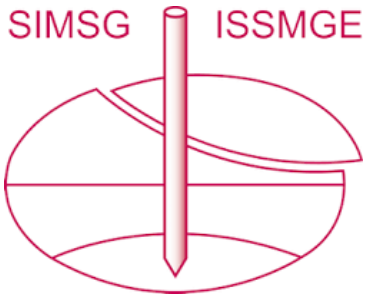

This paper was downloaded from the Online Library of the International Society for Soil Mechanics and Geotechnical Engineering (ISSMGE). The library is available here:

https://www.issmge.org/publications/online-library

This is an open-access database that archives thousands of papers published under the Auspices of the ISSMGE and maintained by the Innovation and Development Committee of ISSMGE.

The paper was published in the proceedings of the 2025 International Conference on Bio-mediated and Bio-inspired Geotechnics (ICBBG) and was edited by Julian Tao. The conference was held from May 18th to May 20th 2025 in Tempe, Arizona.